

Investigation of optical wireless systems for indoor broadband networks

Georgia Ntogari*

National and Kapodistrian University of Athens
Department of Informatics and Telecommunications
gntogari@di.uoa.gr

Abstract. Today's home area networks (HANs) are designed to satisfy the expectations of subscribers for access in bandwidth hungry services, such as High Definition TV - Video, Telepresence, 3D Gaming, Virtual Reality and e-Health. To this direction the use of wireless optical systems is examined. A simulation model was developed in MATLAB to compute the impulse response of the optical wireless channel and determine the characteristics and the restrictions imposed by each channel topology. Appropriate equalization and multiple input multiple output (MIMO) techniques were investigated as a means of fighting intersymbol interference and increasing the coverage area and data rate. In an effort to increase the receiver's sensitivity under the intense ambient light noise the use of coherent sources and homodyne detection is proposed. It is shown that coherent optical wireless systems in combination with space-time diversity enable the transmission of data with rates in the order of ~Gb/s. Finally, the implications of the incorporation of a dimming functionality in the light emitting diodes (LEDs) of a visible light communication (VLC) system are investigated.

Keywords: optical wireless networks, coherent detection, equalization, space time block coding, dimming

I. Introduction

As the demand for ultra broadband wireless access home networks constantly increases, the radio frequency spectrum is becoming extremely congested and thus, attention is drawn towards alternative technologies. Indoor infrared wireless communications were first proposed by Gfeller and Bapst [1] and are since attracting growing interest due to the abundance of unregulated bandwidth, which renders them an attractive candidate for high speed data communications. The infrared channel is not without drawbacks, however. In many indoor environments, it is not easy to achieve a high Signal-to-Noise (SNR) ratio, since there may be intense ambient infrared noise [2]. This noise is due to the infrared spectrum components arising from the radiation of tungsten or fluorescent lamps and sunlight. In addition, artificial light introduces significant in-band components for systems operating at bit rates up to several Mb/s and thus induces interference [3], [4]. Moreover, the power constraints on infrared transmitters imposed by eye-safety regulations, may limit the range of these systems. Infrared links are also susceptible to shadowing caused by objects or people positioned between the transmitter and the receiver.

The effect of shadowing can be dealt with, by using non directed configurations, in which the optical link does not depend on the Line Of Sight (LOS) path between the transmitter and the receiver. Compared to LOS systems, non directed configurations suffer from higher path loss and require higher levels of transmitted power and larger photodetecting area at the receiver. The multipath propagation observed, gives rise to intersymbol interference (ISI), which becomes critical at high data rates. Nevertheless, to date, the non directed configurations, have received great interest from the research community, and a number of experimental links has been reported covering bit rates up to 50 Mb/s [5].

Optical wireless communications with (light emitting diodes (LEDs) emitting in the visible spectral range has recently gained increasing attention and is commonly referred to as visible-light communications (VLC) [6]-[9]. In some use cases, LEDs in VLC systems serve a dual role in providing both illumination and wireless connectivity [8]. The

* Dissertation advisor: Thomas Spicopoulos, Professor.

pioneering idea of using white LEDs lighting systems for communication is attributed to the research group of Nakagawa [8]. Phosphorescent white LEDs have a limited modulation bandwidth ($\sim 2\text{MHz}$), however, by placing a blue optical filter in front of the receiver, the modulation bandwidth can be extended to 20MHz [10]. Using discrete multitone (DMT) modulation [11], VLC systems can provide $>200\text{Mb/s}$ transmission rates with commercial high-power lighting LEDs [12]. Dimming is an essential functionality of modern lighting systems. In the case of LEDs, pulse-width modulation (PWM) seems to constitute the most effective means of accurately controlling LED illumination without incurring color rendering of the emitted light [13], [14].

The objective of this work is to examine the capacity limits of non directed indoor infrared wireless systems assuming different transmitter and receiver configurations in combination with appropriate equalization and multiple input multiple output (MIMO) techniques. In addition, the potential of MIMO coherent optical wireless systems is examined. Finally, the possibility of combining PWM dimming with VLC, based on DMT, on the physical layer is considered both analytically and numerically.

II. Results and Discussion

In order to evaluate the effect of different transmitter-receiver configurations on the performance of a wireless infrared link, a tool that computes the impulse response of the infrared channel for each configuration, based on the modified Monte Carlo method [15], was developed in MATLAB. For the simulations a medium-sized office room, depicted in the inset of Fig. 1 was considered. Table I, outlines the basic configuration parameters for the simulation. In the table, ρ_{north} , ρ_{south} , ρ_{east} , ρ_{window} , ρ_{ceiling} and ρ_{floor} denote the reflectivities of the corresponding surfaces of the room, L_x , L_y and L_z are the room dimensions along the x , y and z axis respectively, depicted in the inset of Fig. 1 and HPSA is the half power semi angle of the transmitter, which is related to the order m of the transmitter radiation pattern through $m = -\ln 2 / \ln(\cos(\text{HPSA}))$. Two transceiver configurations were considered [16]. In the first configuration, classified as vertically oriented, i.e. T1R1, the main lobe of the transmitter and the receiver is directed upwards, towards the ceiling. In the second one, classified as horizontally oriented, i.e. T8R8, some of the lobes are also directed parallel to the ceiling, potentially offering a LOS path and possibly higher coverage.

Table I
Configuration Parameters

PARAMETERS	T1R1	T8R8
Room		
(L_x, L_y, L_z)	(5.5, 7.5, 3.5)	(5.5, 7.5, 3.5)
ρ_{east}	0.3	0.3
ρ_{south}	0.56	0.56
ρ_{north}	0.3	0.3
ρ_{window}	0.04	0.04
ρ_{ceiling}	0.69	0.69
ρ_{floor}	0.09	0.09
Transmitter		
HPSA	$1 \times 60^\circ$	$6 \times 30^\circ + 2 \times 30^\circ$
Azimuthal separation	0	$6 \times 45^\circ$
elevation	$1 \times 90^\circ$	$6 \times 0^\circ + 2 \times 90^\circ$
position	(2, 4, 1.5)	(2, 4, 1.5)
Receiver		
FOV(ϕ_c)	60°	31°
Position	NW-SE diagonal height: 0.8m	NW-SE diagonal height: 0.8

For the T1R1 configuration, the transmitter has a first order Lambertian pattern and is oriented vertically towards the ceiling. The receiver is a pin photodetector of area $A_{\text{det}} = 1\text{cm}^2$ with an optical concentrator having cutoff angle of 60° and refractive index $n_c = 1.44$, while the optical filter has a bandwidth $\Delta\lambda = 50\text{nm}$. For the T8R8 configuration the transmitter uses six equal power 30° HPSA transmit beams equally spaced in the horizontal plane and two such identical beams pointing straight up. The receiver uses eight optical concentrators with cut-off angles 31° , seven of which are horizontally oriented and one is pointing straight up. The power collected from each receiver is added together to obtain the total

received power. The transmitter has a center wavelength of 806nm and is located at a height of 1.5 m, near the center of the room. In order to incorporate the effect of the ambient light noise in the room under investigation, eight incandescent lamps were considered at the ceiling and the west wall of the room was assumed to be a window (in order to account for the sunlight) as is depicted in the inset of Fig. 1.

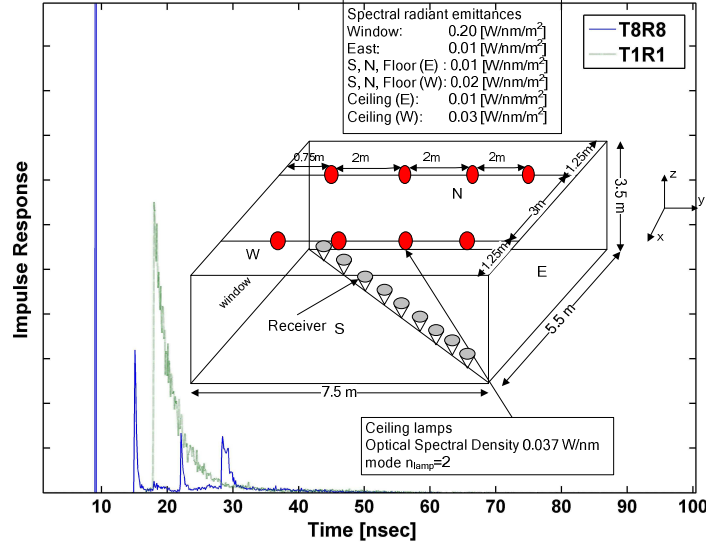


Fig. 1. Impulse response of the optical wireless channel for configurations T8R8 and T1R1.

Taking into account the previously described system parameters, the impulse response was calculated for all the receiver positions along the south-east north-west diagonal of the room and it is depicted in Fig. 1 for the two configurations T1R1 and T8R8. It is deduced that both channels introduce time dispersion, which for high data rates can lead to severe ISI and hence to performance degradation. The T8R8 configuration is bound to induce higher ISI for bit rates $>100\text{Mb/s}$ than T1R1, since the corresponding time dispersion is $>20\text{nsec}$. To this end, the employment of appropriate equalization schemes, i.e. linear (LE) and decision feedback equalization (DFE) was proposed as well as the use of multicarrier schemes, i.e. DMT with MIMO.

A. Equalization schemes for diffuse IR systems

In an effort to mitigate the effects of ISI, several detection schemes have been proposed [5]. In the case of the unequalized system, the SNR is given by [17]:

$$SNR_U = \min_{(i,j)} \left\{ \left\langle \frac{(m_i - m_j)^2}{2N_0} \right\rangle \right\} \quad (1)$$

where m_i is the received signal power when symbol i is transmitted and N_0 the ambient light noise power. In the presence of ISI, for a symbol transmitted at time $t_0=0$, one needs to calculate the values of SNR_U considering the adjacent symbols at $\pm kT$, $k \neq 0$. The parameters m_i are calculated using:

$$m_i = P_p \sum_k a_k \left(\frac{1}{T} \int_{-T/2}^{T/2} p(\tau - kT) d\tau \right) \quad (2)$$

where, P_p the peak power, L is the number of the different transmitted symbols a_k according to the modulation scheme of choice ($L=2$ for OOK and $L=4$ for 4-PPM and 4-PAM) and $T=\log_2(L)/R_b$ is the symbol duration while R_b is the bit rate and assuming that the values of the symbol sequence a_k are such that the symbol transmitted at $t_0=0$ corresponds to i . In (2), $p(t)$ is a rectangular pulse $rect(t)$ (height=1 and width= T) passed through a baseband filter which represents the combined effects of the transmitter shaping, the infrared channel

propagation and the photodiode responsivity. The values obtained by (2) are averaged with respect to the adjacent symbols at $\pm kT$, $k \neq 0$.

The optimum system performance in terms of SNR is obtained when the receive filter is matched to $p(t)$ and is defined as the Matched Filter Bound (MFB) given by [17]:

$$SNR_{MFB} = \frac{P_p}{N_0} \int_{-\infty}^{+\infty} M(f) df \quad (3)$$

where

$$M(f) = \frac{1}{S_n(f)} \left| \int_{-\infty}^{+\infty} p(t) e^{j2\pi ft} \right|^2 \quad (4)$$

In (3), $M(f)$ is the frequency spectrum of the matched filter's output pulse. Alternatively, LE or DFE equalization schemes are suboptimal strategies for detecting signals in the presence of ISI, their primary advantage being a reduction in complexity. For the LE equalizer, the SNR is given by [17]:

$$SNR_{LE} = \frac{P_p}{N_0} \left(\int_{-1/2T}^{1/2T} \frac{df}{S(f)} \right)^{-1} \quad (5)$$

while for the DFE, the SNR becomes [17]:

$$SNR_{DFE} = \frac{P_p T}{N_0} \exp \left(T \int_{-1/2T}^{1/2T} \ln[S(f)] df \right) \quad (6)$$

The spectrum $S(f)$ is given by:

$$S(f) = \frac{N_0}{P_p T} + \frac{1}{T^2} \sum_k M \left(f + \frac{k}{T} \right) \quad (7)$$

The transmit power equals 0.6W and the bit-rate of the system under examination is 100 Mbps. Three modulation schemes were investigated, 4-PPM (pulse position modulation), OOK (on-off keying) and 4-PAM (pulse amplitude modulation). The electrical SNR obtained for the configurations T1R1 and T8R8 is depicted in Fig. 2 and Fig. 3 respectively, for 4-PAM which outperforms OOK and 4-PPM [18], [19], when different equalization schemes are employed.

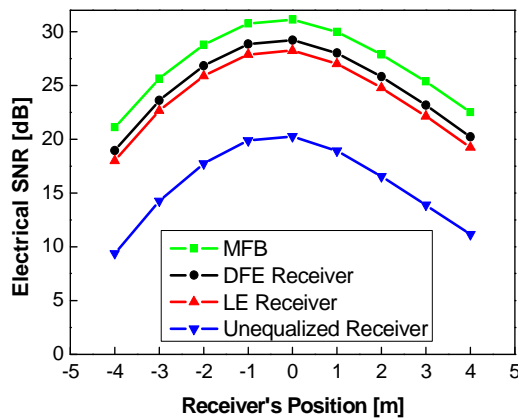


Fig. 2. SNR for T1R1 when 4-PAM is employed.

In Fig. 2 according to the MFB curve, the SNR cannot exceed the value of 30 dB at the center of the room whereas near the corners it does not drop below 20 dB. The DFE and LE schemes improve the performance of the unequalized system by almost 9 and 8 dB respectively.

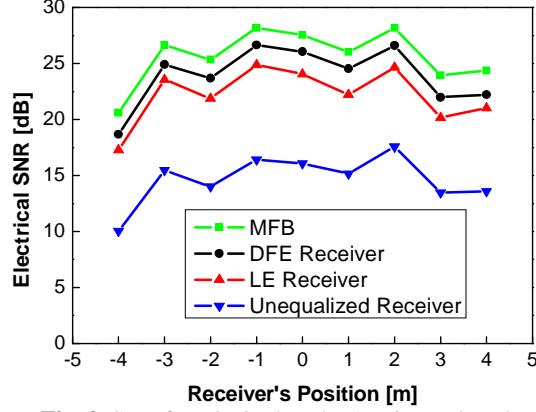


Fig. 3. SNR for T8R8 when 4-PAM is employed.

Better coverage can be obtained using the T8R8 transmitter/receiver configuration. The values of the SNR obtained at different receiver positions, are depicted in Fig. 3. Comparing these values with the ones in Fig. 2 it is deduced that there are no large variations in the values of the SNR and hence, the system performance is not expected to vary significantly (except at the edges of the room).

As in the case of T1R1, both the LE and DFE equalization techniques significantly improve the system performance. For example, if one excludes the SNR values obtained at receiver positions near the two edges of the diagonal, the SNR for T8R8 is higher than 20dB implying a BER much less than 10^{-14} . The worst case SNR is again obtained at the edge of the room and for the case of the equalized schemes is approximately the same as those obtained by T1R1. The variations in the SNR values at different positions along the main diagonal of the room can be interpreted in combination to the impulse response obtained for both configurations, see Fig. 1. It is deduced that in the T8R8 impulse response four peaks are observed while in the T1R1 only one. This can be attributed to the horizontal transmit and receive lobes of the T8R8 configuration and it is the reason for the different shapes of the SNR distribution between T8R8 and T1R1. These results seem to indicate that the T8R8-4-PAM configuration can carry $\geq 100\text{Mb/s}$ (Fast Ethernet type) data rates in almost every point in the room and should be considered favorably as a potential hot spot for future indoor WLANs.

B. Diversity schemes for diffuse infrared wireless systems

This section provides a framework for the performance evaluation of an N MIMO DMT M -QAM (quadrature amplitude modulation) system. It will be shown that using multiple transmitter arrangements in diffuse optical wireless is interesting, since the power requirements per transmitter can be reduced, while system performance can be enhanced. Alamouti-type Space Time Block Coding (STBC) [20] and repetition coding is investigated and compared to Single Input Single Output (SISO) and Maximum Ratio Combining (MRC) [21] taking into account the channel's frequency response as well as the noise distribution throughout the simulation room. In order to mitigate the effects of the channel's frequency response, which is necessary for STBC, DMT modulation with QAM is used.

Assuming Q transmitters the optical power of the q^{th} transmitter is written as:

$$P^q(t) = \frac{A}{Q} \text{Re} \left\{ \sum_{k=-\infty}^{+\infty} \sum_{n=1}^{N-1} s_{k,n}^q e^{j2\pi f_n t} p(t-kT) \right\} + \frac{P_{DC}}{Q} \quad (8)$$

where A is the amplitude of the DMT waveform, $p(t)$ is the QAM pulse shape, $s_{k,n}$ is the k^{th} QAM symbol transmitted at the n^{th} subcarrier channel centered around $f_n=n/T$, T is the DMT signal duration and P_{DC} is a DC power level added to ensure that the optical power is always positive. The symbols $s_{k,n}=a_{k,n}+jb_{k,n}$ take their values from a QAM constellation. Hence, the possible values of $a_{k,n}$ and $b_{k,n}$ are given by $2u-(M^{1/2}+1)$ where $1 \leq u \leq M^{1/2}$ and M is the number of QAM distinct symbols in the constellation assumed to be a power of 2, i.e. $M=2^L$. Usually L is an even number. The duration of the QAM symbol is given by $T=\log_2(M)/R_b$ where R_b is the bit rate. The pulses $p(t)$ are assumed ideal rectangular pulses, such that $p(t)=1$ for $0 \leq t \leq T$ and $p(t)=0$ otherwise. Note that equation (8) assumes that the DC

subcarrier at $f_0=0$ is not modulated, as in [22] in order to avoid interference problems from electronic ballasts.

In the absence of clipping and since $P(t) \geq 0$ one can choose the amplitude A such that $\min\{P(t)\} \geq 0$. Taking into account that:

$$\left| \operatorname{Re} \left\{ \sum_{n=1}^{N-1} s_{k,n} e^{j2\pi f_n t} \right\} \right| \leq \left| \sum_{n=1}^{N-1} s_{k,n} e^{j2\pi f_n t} \right| \leq \sum_{n=1}^{N-1} |s_{k,n}| \quad (9)$$

and that $\max\{|s_{k,n}|\} = 2^{1/2}[(M)^{1/2} - 1]$, it is easy to show that the following choice for A ,

$$A = \frac{P_{DC}}{\sqrt{2}(\sqrt{M} - 1)(N - 1)} \quad (10)$$

At the receiver the SNR for the m^{th} subcarrier is computed by:

$$\text{SNR}_m = (RA/2Q)^2 V_m / N_0 \quad (11)$$

where R is the receiver's responsivity factor, N_0 the noise power and V_m the channel matrix which depends on the selected scheme. For Alamouti STBCs $V_m = \sum_{p,q} |h_{p,q}(f_m)|^2$ while for repetition coding $V_m = (\sum_{p,q} |h_{p,q}(f_m)|)^2$ where $h_{pq}(f)$ is the channel transfer function between the p^{th} receiver and the q^{th} transmitter². The Bit Error Rate (BER) is computed by [23]:

$$P_e = \frac{4}{N} \sum_{n=1}^{N-1} \frac{\sqrt{M} - 1}{\sqrt{M} m} Q \left(\sqrt{\frac{3mM}{M-1} \text{SNR}_n} \right) \quad (12)$$

where $m = \log_2 N$.

The configuration used in the simulations is T1R1 for the room depicted at the inset of Fig.1. The noise power distribution was computed assuming irradiance of eight incandescent lamps and sunlight. The BER was computed for various receivers' positions along the main diagonal of the room (NW to SE) at a height of 0.8 m from the floor. The transmitters are positioned along the main diagonal at equal distances from the center and 1.0 m above the floor. For the single input schemes (SISO and MRC) one transmitter was assumed, positioned in the center of the room again at a height of 1.0 m.

Three MIMO schemes were considered [24]; the first employing two transmitters and one receiver (2×1), the second two transmitters and two receivers (2×2) using repetition coding and STBC, whereas the third one transmitter and two receivers (MRC). These schemes are compared to a SISO system. In multiple receiver arrangements, the spacing between the receivers was equal to 35 cm. The results were obtained for a 100 Mb/s, 16-QAM/DMT of 32 subcarriers, with $P_{DC} = 0.6\text{W}$.

Fig. 4 shows the values of the BER as a function of the distance d from corner A of the room (NW corner). As seen by the figure, the 2×1 Alamouti and the SISO schemes have a large BER at small values of d , in which case the receiver is situated near the window of the room (see Fig. 1) and hence the power of the ambient light noise is high. Regarding the multiple receiver systems, one notices that MRC is generally better than the 2×1 and SISO, a fact that is observed in radio wireless systems as well [20]. On the other hand, both the repetition coding and the Alamouti 2×2 systems outperform the MRC, leading to a significant performance enhancement.

It is interesting to observe that the 2×2 and 2×1 systems achieve their optimum performance near $d \approx 7.5\text{m}$ while the minimum BER for single transmitter schemes is obtained near the center of the diagonal of the room. This can be explained since the SNR is not the same in the four systems under consideration. In contrast to SISO and 2×1 , in the case of MRC and 2×2 systems there are two receivers, each one adding a slightly different noise component. The figures also illustrate that MIMO schemes do not always guarantee a performance enhancement especially if STBC is used. Interestingly enough however, repetition coding compares more favourably to MRC as illustrated by Fig. 4. In addition repetition coding outperforms STBC and this is not surprising since the systems considered use direct detection. However, multiple transmitter arrangements have the advantage of using lower power transmitters, relaxing the power constraints due to eye or skin safety.

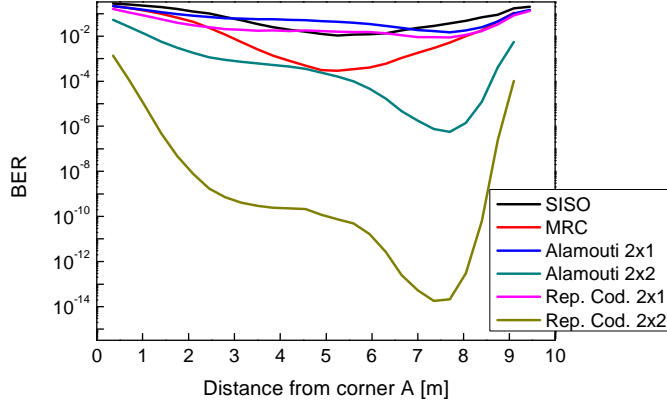


Fig. 4. Comparison of SISO, MRC, Alamouti 2×1 and 2×2, and Repetition Coding 2×1 and 2×2 schemes for various receiver positions along the main diagonal of the room.

C. Diversity schemes for coherent LOS infrared wireless systems

Inspired by the fact that unlike direct detection, in coherent detection the photocurrent is proportional to the incident electric field we will examine in this section the potential of STBC schemes as a means of further improving the coverage and data rate of coherent indoor optical LOS links. To this end, analytic formulas for the BER are derived for two Alamouti schemes and are compared to a SISO system. The BER performance of the system is realistically examined taking into account both thermal and shot noise, although ideal coherent receivers are usually considered shot noise limited for a sufficient local oscillator (LO) power. It is shown that Alamouti STBC may increase the capacity of coherent LOS IR systems, improve their coverage and decrease the required optical power at the transmitter.

The SISO coherent IR system uses of a phase-shift-keying (PSK) modulator which imprints the information on the phase of the optical carrier wave emitted by the laser source. The emitted light is collimated and uniformly illuminates the coverage area through a holographic diffuser [25]. At the receiver homodyne detection is employed using a 90° optical hybrid followed by two balanced photodetectors [26]. The received and LO fields are considered linearly polarized in orthogonal directions.

The approximate closed form formula for the BER in the case of M -level PSK modulation and a 2×1 Alamouti scheme is given by [23]:

$$P_e^{2 \times 1} = \frac{2}{\log_2 M} Q \left(\sqrt{2 \sin^2 \left(\frac{\pi}{M} \right) \log_2 M \frac{\|\mathbf{H}\|^2}{\sigma^2}} \right) \quad (13)$$

where $Q(x)$ is the Q function and σ^2 is the total noise power calculated by multiplying the total noise PSD given by with the bit rate, R_b , of the system and \mathbf{H} is a 2×2 array with channel coefficients given by [27]:

$$H_{pl} = 2R \sqrt{\frac{P_{LO} P_T A_{eff}^{(pl)}}{2A_{cov}}} e^{j(kd_{pl} - \phi_{LO})} \quad (14)$$

where R is the receiver's responsivity, P_{LO} and ϕ_{LO} is the optical power and phase of the LO at the receiver, P_T is the average transmitted optical power, $A_{eff}^{(pl)}$ the effective receiver area, A_{cov} the total coverage area of the system and d_{pl} the distance between transmitter p and receiver l . The distance between the receivers for the 2×2 system was taken equal to 0.07m, the total transmitted optical power is $P_T=20$ mW and the LO power is $P_{LO}=5$ mW.

Following a similar approach, it is also possible to derive the BER in the case of a repetition coding 2×1 scheme. It can easily be shown that formula still holds if one replaces $\|\mathbf{H}\|=|H_{11}|^2+|H_{21}|^2$ by $|H_{11}+H_{21}|^2$. Using, it is possible to show that:

$$|H_{11} + H_{21}|^2 = |H_{11}|^2 + |H_{21}|^2 + 4R^2 \frac{P_{LO} P_T A_{eff}}{A_{cov}} \cos(k(d_{11} - d_{21})) \quad (15)$$

Equation (15) suggests that, since d_{11} and d_{21} are much larger than the wavelength $\lambda=c/f_0$, then the error probability in may undergo large fluctuations even for small changes in the terminal position

The system under investigation is located within a room of dimensions $6 \times 6 \times 3$ m like in [25]. Using the equations outlined previously the BER for all three configurations was obtained at multiple receiver positions. A BPSK scheme was considered and the bit rate is taken at $R_b=1$ Gb/s. The transmitters employed in the STBC schemes emit half the power than the transmitter employed in SISO. The dominant noise source in the system under study is the LO shot noise with a PSD of $\cong 53$ pA $\sqrt{\text{Hz}}$ whereas the PSD of the ambient light noise and the thermal noises calculated in the same way as in [24] turn out to be $\cong 0.005$ pA $\sqrt{\text{Hz}}$ and $\cong 5$ pA $\sqrt{\text{Hz}}$ respectively.

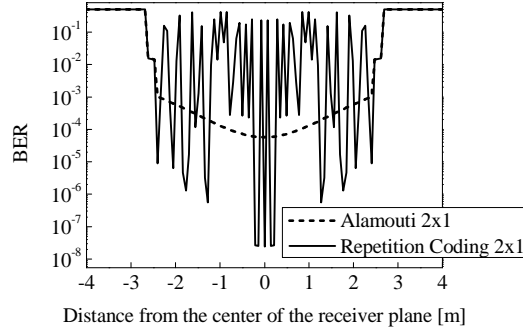


Fig. 5. BER along the main diagonal on the receiver plane for an Alamouti and a repetition coding 2×1 scheme.

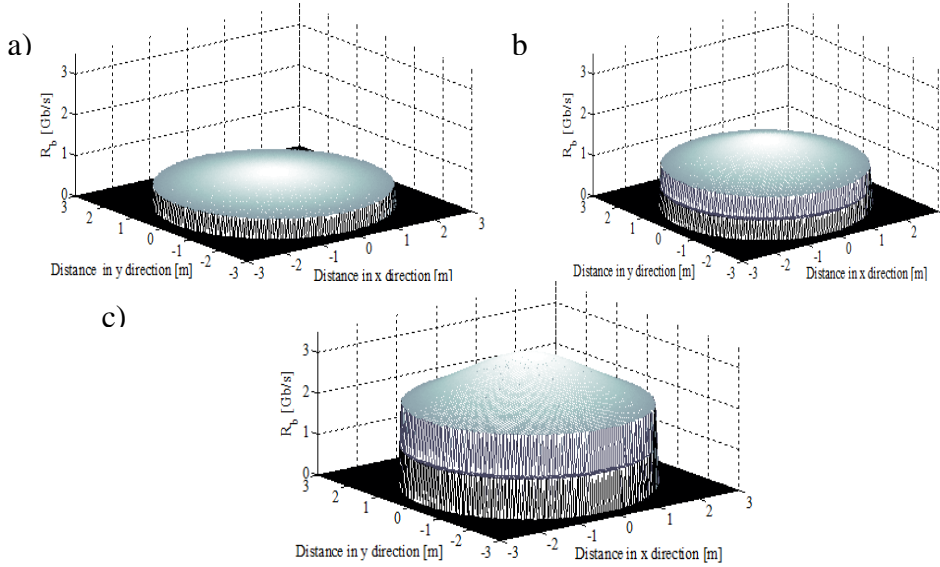


Fig. 6. Maximum R_b value throughout the room for the a) SISO scheme, b) 2×1 Alamouti STBC and c) 2×2 Alamouti STBC when a BER of 10^{-3} is assumed.

In Fig. 5 we show the BER computed along the main diagonal on the receiver plane for Alamouti and repetition coding 2×1 . It is interesting to observe that while for some receiver positions the BER is lower ($\sim 10^{-7}$) than the one obtained using the Alamouti scheme, for other positions which are in close proximity, the BER is extremely high ($\sim 10^{-1}$) rendering communication impossible. These variations are attributed to the cosine term appearing in (15). The obtained results demonstrate that a coherent optical wireless system employing repetition coding may not provide reliable communication due to these large BER fluctuations.

The SISO, 2×1 and 2×2 STBC systems were also evaluated in terms of the achievable bit rate. To this end, the maximum bit rate was computed for the various receiver positions assuming a target BER value, equal to 10^{-3} . The results are depicted in Fig. 6a), b) and c). It is shown that the SISO scheme can reach data rates as high as 0.6Gb/s while in less favorable positions the achieved bit rate is between 0.2 and 0.4Gb/s. The use of STBC schemes increases the maximum bit rate to 1.5Gb/s and 3Gb/s for the 2×1 and 2×2 schemes

respectively. The above results demonstrate the usefulness of OSTBC in gigabit coherent IR wireless systems in terms of the achievable bit rate.

D. PWM dimming for DMT-based visible light communication systems

The proposed VLC system is illustrated in Fig. 7 [28].

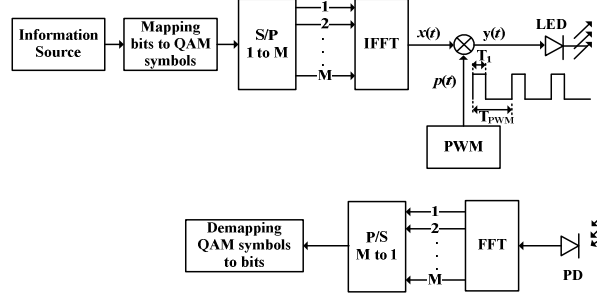


Fig. 7. Basic blocks of a PWM-DMT VLC system.

The data bits to be transmitted are converted into a sequence of symbols, using a QAM constellation mapper. The produced symbols are fed to a serial to parallel (S/P) converter and undergo an inverse Fourier transform (IFFT) operation to form the multicarrier signal $x(t)$. The generated multicarrier signal is multiplied by a periodic PWM pulse train $p(t)$ with a duty cycle of $d = T_1/T_{P_{PWM}}$, where T_1 is the duration of the PWM pulse and $T_{P_{PWM}}$ is the period of the PWM signal. The dimming level δ is determined by $\delta = 1-d$. The resulting composite signal $y(t)=x(t)p(t)$ is the driving current of the LED. The transmitted signal $y(t)$ impinges on the photodiode receiver, undergoes an FFT operation and the resulting baseband signal is fed to a parallel to serial converter. The generated symbols are estimated using appropriate detection schemes.

The PWM signal is periodic and can therefore be expressed in terms of a Fourier series,

$$p(t) = \sum_{n=-\infty}^{\infty} C_n e^{j2\pi n t / T_{P_{PWM}}} \quad (16)$$

where C_n are the Fourier coefficients of $p(t)$. If $p(t)$ is rectangular, then C_n will be exhibiting a sinc-like dependence with respect to n . Therefore, one can show that the spectrum of the signal waveform $y(t)$, which is in general given by:

$$Y(f) = \int_{-\infty}^{+\infty} dt y(t) e^{-j2\pi f t} \quad (17)$$

can be expressed as:

$$Y(f) = \sum_{n=-\infty}^{+\infty} C_n X(f - n f_{P_{PWM}}) \quad (18)$$

According to (18), and much as in the case of digital signal sampling, the spectrum of $y(t)$ is comprised of a weighted sum of displaced versions of the original spectrum $X(f)$. In the case of a DMT signal, $X(f)$ can be assumed to be contained inside $f \in [-B B]$, where B is approximately the frequency of the highest subcarrier f_{M-1} . Consequently, if the PWM rate $f_{P_{PWM}}$ is chosen to be twice the bandwidth B of the DMT signal ($f_{P_{PWM}} \geq 2B \cong 2f_{M-1}$) then the spectral components $C_n X(f - n f_{P_{PWM}})$ will experience no aliasing. In the case of the PWM waveform considered in Fig. 8a), $C_0 = T_1/T_{P_{PWM}} = d$, and consequently, when $f_{P_{PWM}} \geq 2B \cong 2f_{M-1}$,

$$Y(f) = X(f)d \quad (19)$$

for $f \in [-B B]$. According to (19), the spectrum remains unchanged in shape upon dimming, as suggested by Fig. 8b), and hence, if $F = f_{P_{PWM}}/f_{M-1} \geq 2$, one expects no interference between the subcarriers. This is an important conclusion and will be used to justify the enhanced system performance obtained for $F \geq 2$.

In order to gain a better insight on the system's performance the BER was calculated. For this analysis we resorted to Monte Carlo simulations. The system performance was investigated in terms of the achieved BER for various dimming levels. Again, $M = 32$ and

$N = 16$ are considered, with the last subcarrier positioned at 500 kHz. The employed detection scheme takes into account the self-interference term and should produce no errors in the case of infinite signal to interference ratio. However, it requires knowledge of the timing as well as the dimming level at the receiver. Taking into account the ambient light noise the mean value of the BER was computed and it is shown in Fig. 9 for a synchronized system. An SNR of 45 dB, corresponding to a transmit optical power of 0.6W and a noise power spectral density of $\sim 10^{-11}$ A²/Hz, higher than in [29] was assumed, and two dimming levels (80% and 20%) were considered. The mean BER reaches low values in the region where the relative rate F is approximately larger than 2.

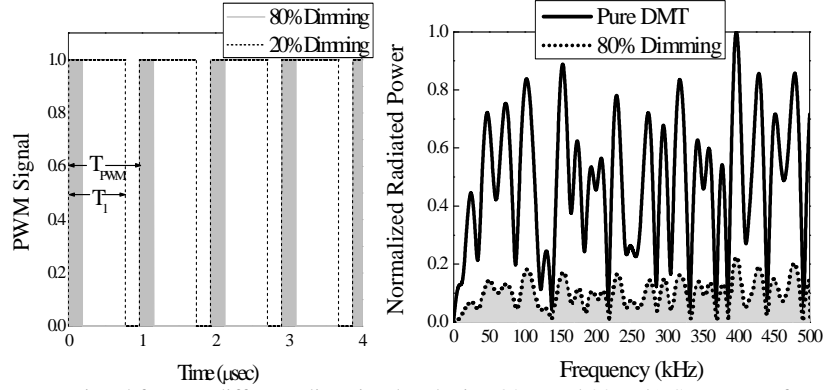


Fig. 8. a) PWM signal for two different dimming levels, i.e. 80% and 20%. b) Spectrum of composite PWM-DMT signal and pure DMT signal for $F=2$.

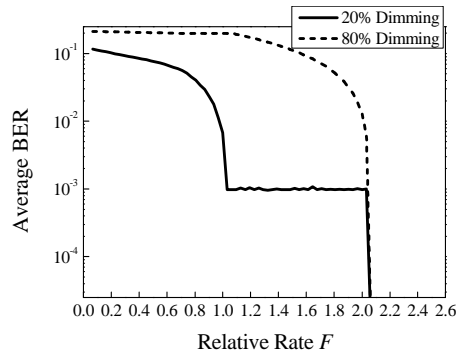


Fig. 9. Mean BER for synchronized signal, detection scheme B for various dimming levels with noise.

There is also another important implication regarding the illumination performance of the system. The optical power emitted by the LED is proportional to $y(t)$, and (19) suggests that in the frequency regime $|f_L| < 200$ Hz, where the human eye may sense optical power variations [30], incorporation of PWM will not distort the spectrum of the original signal. Consequently, PWM will not introduce any significant additional flickering.

To further investigate whether LED light flickering is induced in a PWM/DMT VLC system, we consider the low frequency component $y_{LOW}(t)$ corresponding to the part of the spectrum $Y(f)$ residing inside $f \in [-f_L, f_L]$,

$$y_{LOW}(t) = \int_{-f_L}^{f_L} Y(f) e^{-j2\pi f t} dt \quad (20)$$

The flickering factor C_F , defined as:

$$C_F = \frac{\max\{|y_{LOW}(t)|\} - \min\{|y_{LOW}(t)|\}}{Y(0)} \quad (21)$$

where $Y(0)$ is the DC component of the signal $y(t)$, is a measure of the LED light flickering.

The values of the average C_F were calculated numerically based on Monte Carlo simulation. 100 iterations were considered, and on each, 31 QAM symbols s_m were randomly chosen, one for each active subcarrier. The DMT waveform $x(t)$ was then calculated and was multiplied by the PWM signal $p(t)$ to estimate $y(t)$. The spectrum $Y(f)$ of

$y(t)$ was calculated using a discrete Fourier transform (DFT) in the low frequency regime, $f \in [-f_L, f_L]$. Performing an inverse DFT according to (20), we then calculate $y_{\text{LOW}}(t)$ and estimate the average flickering factor C_F obtained from each of these 100 waveforms. In Fig. 10 the relative deviation of flickering factors with respect to the undimmed case, are depicted, for $\delta = 80\%$ and $\delta = 20\%$. This ratio appears to be very low, in the order of $\cong 10^{-6}$, and hence no perceivable LED light flicker is expected.

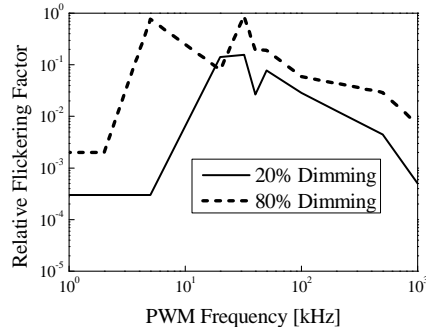


Fig. 10. Relative flickering factor for different PWM line rates when 20 and 80% dimming is considered.

III. Conclusions

In this work, the potential of indoor optical wireless systems was examined for data rates higher than 100 Mb/s. It was shown that diffuse infrared systems can reliably carry traffic of 100Mb/s inside a medium size room when appropriate equalization techniques are employed. In addition MIMO optical wireless schemes were investigated for intensity modulated systems based on STBC and repetition coding. It was shown that STBC does not provide significant performance gains while in contrast, repetition coding based MIMO could be used to relax the power constraints in future optical wireless LANs. On the other hand, STBC techniques can be used to increase the capacity of coherent optical wireless systems, improve their coverage and decrease the required optical power at the transmitter. In an effort to further enhance the performance of indoor IR systems the use of more than two transmit elements ($N_T > 2$) would also constitute an interesting and viable solution. Such arrangements could further alleviate the high power requirements of IR systems. An important implementation issue to consider in these systems is the estimation of the channel coefficients required in symbol demodulation. Another issue to consider is the incorporation detection schemes that can allow arbitrary signal/local oscillator polarizations. These issues should be the subject of future investigation.

The implications of PWM dimming in the performance of a DMT-based VLC system were also presented. The influence of PWM in the spectrum of the DMT waveform was analyzed both theoretically and numerically. Closed-form formulas were derived enabling the estimation of the signal-to-interference ratio at the receiver. Numerical Monte Carlo simulations were used to estimate the BER of the system. The results showed that reliable communication is only possible when the PWM samples the DMT waveform at a rate faster than twice the highest subcarrier frequency of DMT. For slower PWM rates, there is significant spectral aliasing leading to prohibitively large subcarrier interference. The analysis was extended to account for ambient light noise and the main conclusions remained unaltered. Since the PWM rate should remain well within the 3dB LED bandwidth, the need to use a PWM signal twice as fast as the frequency of the last subcarrier ultimately sets a limit on the amount of information that can be transmitted over the system. The results also showed while there is no inherent need to synchronize the PWM and the DMT waveforms, synchronizing DMT to PWM is making the BER performance much less independent of clock jitter and the like. In the case of “oversampled” DMT we also showed that combining DMT and PWM does not increase the inherent flicker of PWM-dimmed light.

References

- [1] F.R. Gfeller and U. Bapst, “Wireless in-house data communication via diffuse infrared radiation,” *Proc. IEEE*, vol. 67, pp. 529–551, November 1979.

- [2] A.C. Boucouvals, "Indoor ambient light noise and its effect on wireless optical links," *Proc. Optoelectronics IEE*, vol. 143, pp. 334–338, December 1996.
- [3] A. J.C. Moreira, R.T. Valadas, and A.M. de Oliveira Duarte, "Characterization and modeling of artificial light interference in optical wireless communication systems," *Proc. IEEE Personal Indoor and Mobile Radio Communications (PIMRC '95)*, vol. 1, pp. 326–331, September 1995.
- [4] A. J.C. Moreira, R.T. Valadas, and A.M. de Oliveira Duarte, "Optical interference produced by artificial light," *Wireless Networks.*, vol. 3, pp. 131–140, May 1997.
- [5] G.W. Marsh and J.M. Kahn, "50-Mb/s diffuse infrared free-space link using on-off keying with decision feedback," *IEEE Photonics Technology Letters*, vol. 6, pp. 1268–1270, October 1994.
- [6] D. C. O'Brien, L. Zeng, H. Le-Minh, G. Faulkner, O. Bouchet, S. Randel, J. Walewski, J. A. R. Borges, K.-Di. Langer, J. Grubor, K. Lee and E. T. Won, "Visible Light Communications", White-Paper in Wireless World Research Forum 20 (WWRF 20), Ottawa, Canada, Apr. 2007
- [7] H.Le-Minh, D. C. O'Brien, L. Zeng, O. Bouchet, S. Randel, J. Walewski, J. A. R. Borges, K.-Di Langer, J. Grubor, K. Lee and E. T. Won, "Short-range Visible Light Communications", Proceedings of Wireless World Research Forum 19 (WWRF 19), Chennai, India, Nov. 2007.
- [8] T.Komine, Y. Tanaka, S. Haruyama and M. Nakagawa, "Basic Study on Visible-Light Communication using Light Emitting Diode Illumination," *Proc. of the 11th Int. Symposium on Personal, Indoor and Mobile Radio Communications (PIMRC 2000)*, London, US, pp. 1325-1329, 2000.
- [9] J. Grubor, O. C. Gaete Jamett, J. W. Walewski, S. Randel, K. -D. Langer, "High-Speed Wireless Indoor Communication via Visible Light," *ITG Fachbericht*, 2007, pp.203-208.
- [10] [12] S. Randel, F. Breyer, S. C. J. Lee and J. W. Walewski, "Advanced modulation schemes for short-range optical communications," *Journal of Selected Topics in Quantum Electronics*, September/October 2010.
- [11] [13] J. A. C. Bingham, "Multicarrier modulation for data transmission: An idea whose time has come," *IEEE Communications Magazine*, vol. 28, pp. 5-14, May 1990.
- [12] [14] J. Vucic, C. Kottke, S. Nerreter, A. Buttner, K.-D. Langer, J. W. Walewski, "White Light Wireless Transmission at 200+ Mb/s Net Data Rate by Use of Discrete-Multitone Modulation," *IEEE Photonics Technology Letters*, Vol. 21, Issue 20, pp. 1511 – 1513, Oct.15, 2009.
- [13] [15] Y. Zhang, Z. Zhang, Z. Huang, H. Cai, L. Xia and J. Zhao, "Apparent brightness of LEDs under different dimming methods," *Proc. SPIE*, Vol. 6841, 2007.
- [14] [16] S. Muthu, F. J. Schuurmans, M. D. Pashley, "Red, Green, and Blue LED based white light generation: Issues and control," 37th Annual IEEE-IAS meeting, Vol. 2, 327-333, 2002.
- [15] F.J. Lopez-Hernandez, R. Perez-Jimenez, and A. Santamaria, "Modified Monte Carlo scheme for high-efficiency simulation of the impulse response on diffuse IR wireless indoor channels," *Electronics Letters*, vol. 34, pp. 1819–1820, September 1998.
- [16] J.B. Carruthers and J.M. Kahn, "Angle diversity for non-directed wireless infrared communication," *IEEE Trans. On Comm.*, vol. 48, pp. 960–969, June 2000.
- [17] J.G. Proakis, *Digital Communication*, 4th ed., New York: Mc Graw-Hill, 1995, pp. 601-626.
- [18] G. Ntogari, T. Kamalakis and T. Spicopoulos, "Performance Analysis of Non-Directed Equalized Indoor Optical Wireless Systems", *CSNDSP08 Graz, Austria*, 2008.
- [19] G. Ntogari, T. Kamalakis and T. Spicopoulos, 'Performance Analysis of Decision Feedback and Linear Equalization schemes for Non-Directed Indoor Optical Wireless Systems', *Journal of Communications*, Vol 4, No 8, pp. 565-571, 2009.
- [20] S. M. Alamouti, "A Simple Transmit Diversity Technique for Wireless Communications," *IEEE J. Select. Areas Comm.*, vol. 16, pp. 1451-1458, October 1998.
- [21] P. Djahani and J. M. Kahn, "Analysis of Infrared Wireless Links Employing Multibeam Transmitters and Imaging Diversity Receivers", *IEEE Trans. on Comm.*, vol. 48, no.12, pp.2077-2088, December 2000.
- [22] J. Grubor, S. Ch. J. Lee, K.-D. Langer, T. Koonen, and J. W. Walewski, "Wireless High-Speed Data Transmission with Phosphorescent White-Light LEDs," *Proceedings 33rd European Conference and Exhibition on Optical Communication*, Vol. 6, Post-Deadline Papers, PD3.6, 2007.
- [23] E. G. Larsson and P. Stoica, *Space-Time Block Coding for Wireless Communications*, Cambridge University Press 2003.
- [24] G. Ntogari, T. Kamalakis, and T. Spicopoulos, "Performance analysis of space time block coding techniques for indoor optical wireless systems," *IEEE Journal on Selected Areas in Communications*, vol. 27, pp. 1545-1552, 2009.
- [25] M. Jafar, D. C. O'Brien, C. J. Stevens, and D. J. Edwards, "Evaluation of coverage area for a wide line-of-sight indoor optical free-space communication system employing coherent detection," *IET Commun.* vol. 2, pp. 18–26, 2008.
- [26] D.-S. Ly-Gagnon, S. Tsukamoto, K. Katoh, and K. Kikuchi, "Coherent detection of optical quadrature phase-shift keying signals with carrier phase estimation," *Journal of Lightwave Technol.*, vol. 24, no. 1, January 2006.
- [27] G. Ntogari, T. Kamalakis, and T. Spicopoulos, "Analysis of indoor multiple input multiple output coherent optical wireless systems," accepted for publication at *IEEE J. of Lightw. Technol.*, 2011.
- [28] G. Ntogari, T. Kamalakis, J. Walewski, T. Spicopoulos, 'Combining Illumination Dimming Based on Pulse-Width Modulation With Visible-Light Communications Based on Discrete Multitone', *IEEE/OSA Journal of Optical Communications and Networking*, 3 (1), pp. 56-65, 2011.
- [29] J. Grubor, S.Randel, K.-D. Langer, and J. W. Walewski, "Broadband Information Broadcasting Using LED-Based Interior Lighting," *Journal of Lightwave Technology*, vol. 26, no.24, December, 2008.
- [30] IEEE P802.15.7 Standard, "Part 15.7: Wireless Medium Access Control (MAC) and Physical Layer (PHY) Specifications for Visible Light Wireless Personal Area Networks (WPANs)," The Institute of Electrical and Electronics Engineers, Inc. 2009.